frontiers | Frontiers in Earth Science

TYPE Original Research
PUBLISHED 21 September 2022
DOI 10.3389/feart.2022.1019716

OPEN ACCESS

EDITED BY
Junjian Zhang,
Shandong University of Science and Technology, China

REVIEWED BY
Yu Wang,
University of Science and Technology Beijing, China
Huang Zhihuai,
Pearl River Hydraulic Research Institute, China

*CORRESPONDENCE
Huaichang Yu,
yuhuaichanghb@126.com

SPECIALTY SECTION
This article was submitted to Economic Geology,
a section of the journal
Frontiers in Earth Science

RECEIVED 15 August 2022
ACCEPTED 05 September 2022
PUBLISHED 21 September 2022

CITATION
Yu H, Wang G, Zhang Z, Niu R and Cheng G (2022), Experimental study on the effect of prefabricated fissures on the creep mechanical properties and acoustic emission characteristics of sandstone under uniaxial compression. *Front. Earth Sci.* 10:1019716.
doi: 10.3389/feart.2022.1019716

Experimental study on the effect of prefabricated fissures on the creep mechanical properties and acoustic emission characteristics of sandstone under uniaxial compression

Huaichang Yu[1,2]*, Guanqiang Wang[1], Zhongyu Zhang[3], Rui Niu[1] and Guangli Cheng[4]

[1]College of Geosciences and Engineering, North China University of Water Resources and Electric Power, Zhengzhou, China, [2]Henan Province Key Laboratory of Rock and Soil Mechanics and Structural Engineering, Zhengzhou, China, [3]School of Mechanics and Civil Engineering, China University of Mining and Technology, Beijing, China, [4]Beijing Engineering Corporation Limited, Beijing, China

This study investigates the effect of prefabricated fissures on the creep mechanical strength and acoustic emission (AE) characteristics of sandstone. Under the same test conditions, indoor uniaxial compression creep AE tests were performed on intact and artificially fissured sandstone specimens using a rock rheometer and a PCI-II AE tester controlled with an RLJW-2000 microcomputer. The variation characteristics of strain, long-term strength, number of AE events, AE ringing count, AE energy, and RA value of the two specimens were then analyzed to determine the effect of prefabricated fissures on the creep mechanical properties and AE characteristics of sandstone. The results show that under the same stress level, the instantaneous strain, creep strain, and total strain of the prefabricated fissures specimen was larger than the corresponding values of the intact specimen. The prefabricated fissures exhibited the most significant influence on the creep strain of the specimen, followed by the total strain. The fissures showed the least influence on the instantaneous strain of the specimen. Furthermore, the long-term strength of the prefabricated fissures specimen was only 37.5% of that of the intact specimen. Owing to the influence of the prefabricated fissures, the long-term strength of the sandstone was significantly reduced. In engineering practice, fissures should be noted and analyzed for the potential failure of a formation. Moreover, as the stress level increases, the number of AE events of the specimen also increases. The number of AE events and cumulative AE events generated by the prefabricated fissures specimen at various stress levels is significantly higher than the corresponding values of the intact specimen. The maximum ringing count of the prefabricated fissures specimen was 7.3 times that of the intact specimen, and the maximum AE energy was 3.8 times that of the intact specimen. The cumulative AE ringing count was 1.5 times that of the intact specimen, and the cumulative energy was 4.5 times that of the intact specimen. The prefabricated fissures significantly affect the maximum AE ringing count, maximum AE energy, cumulative AE ringing count, and

cumulative AE energy of the specimen. Finally, tensile fissures were the main microcracks generated inside the intact specimen during creep, and shear cracks were secondary. The microcracks generated inside the prefabricated fissures specimen consisted of mixed tension-shear cracks, but mainly consisted of shear cracks with fewer tension cracks. The RA value correlates well with the observed internal microcracks, indicating that the RA value can be used to characterize fractures in sandstone specimens. The RA value has a guiding significance for characterizing the type of internal microcracks in the process of rock creep.

KEYWORDS

sandstone, prefabricated fissures, creep, acoustic emission, uniaxial compression

Introduction

A fissured rock mass is one of the most common and essential geological media in water conservancy, mining, transportation, energy, national defense, and other industries (Vásárhelyi and Bobet, 2000; Haeri et al., 2014). Owing to the rock formation and tectonic movement, joints, and fissures with different scales are present inside the rock mass. The deformation and failure characteristics of a fissured rock mass directly affect the safety and stability of large-scale underground powerhouses, ultra-long hydraulic tunnels, underground energy storage, and underground nuclear waste isolation. It is one of the critical factors that should be considered in engineering design, construction, and long-term operation. Numerous engineering practices show that the fracture and instability of engineering rock mass are mostly caused by the initiation, expansion, and penetration of cracks of various scales in the rock mass under the action of environmental forces. In engineering, processes occurring in a fissured rock mass from the initial deformation to the final rupture and instability constitute a time-dependent and complex non-linear progressive process, and in this process, the rock mass undergoes creep failure. For example, the marble of Jinping I Hydropower Station in China, the gneiss of Xiaowan Hydropower Station, and the granite of the Three Gorges Hydropower Station all show substantial creep deformation and failure characteristics, along with well-developed fissures (Yang et al., 2018). Therefore, investigation of the effect of fissures on the creep characteristics of rock mass is significantly essential research and has very important engineering practical significance for revealing the fracture mechanism of rock mass, evaluating the long-term stability of rock mass engineering, and taking reasonable preventive measures.

Scholars have performed conventional mechanical tests on fissured rock masses to study the effect of fissures on the mechanical characteristics of rock masses. Some researchers used similar materials such as gypsum and cement mortar to fabricate fissured rock masses and conducted laboratory experiments on the mechanics. Feng et al. (2018) conducted uniaxial compression tests on rock-like specimens with two different fissures inclination angles and studied the effect of strain rate on the mechanical behavior of the specimens. Li et al. (2020) conducted uniaxial compression tests on double-fissure-like sandstone specimens and analyzed the fracture failure characteristics and strength loss laws of the specimens under different rock bridge inclination angles. Yi et al. (2021) conducted uniaxial compression tests on rock-like materials with different inclination angles and different numbers of fissures. They analyzed the influence of these variables on the strength and deformation characteristics of the specimen. Chen et al. (2012) systematically studied the influence of fracture connectivity on the uniaxial compression strength, deformation, and fracture characteristics of the rock mass. These studies have enriched the research on the conventional mechanical properties of fractured rock masses in rock-like materials. However, these studies did not take into account fissures in natural specimens.

Furthermore, studies have also been conducted on natural rock specimens with prefabricated fissures via laboratory mechanical test experiments. For instance, Yang and Jing, 2011 conducted uniaxial compression tests on single-fracture brittle sandstone specimens and studied the effects of the length and inclination of the fissures on the strength, deformation, and failure behavior of sandstone materials. Huang and Huang, 2010 conducted uniaxial compression tests on marble with prefabricated fissures and analyzed the influence of the fissures on mechanical characteristics. Lu et al. (2015) conducted a uniaxial compression test on sandstone with a single three-dimensional (3D) surface crack and studied the influence of the geometric parameters of the crack on the strength of the sandstone. These studies have enriched the effect of cracks on mechanical properties of real rock under uniaxial compression. Although effective, these techniques did not include acoustic emissions (AE), which can significantly enhance their findings and application in the field.

Researchers have also combined AE technology to further study the mechanics and AE characteristics of fissured rock masses (Zhu et al., 2019; Song, 2021). Wang et al. (2019)

conducted AE tests on the whole and prefabricated fissured sandstone specimens under uniaxial compression. They analyzed the influence of the prefabricated fissures on the mechanical properties and AE characteristics. Yang et al. (2013) conducted a uniaxial compression test on red sandstone with two non-parallel fissures and used AE monitoring technology to analyze the influence of the fracture inclination on the strength, deformation, and failure characteristics of red sandstone. These studies used AE technology to further explain the mechanical properties of fractured rock masses but have not addressed creep failure in the specimens. They focused on brittle failure rather than plastic and elastic deformation.

Overall, most rocks under stress undergo creep failure due to the constant load for an extended period, leading to a project's instability and eventual catastrophe. This has been shown by various studies on creep AE tests of intact rock specimens. Xu et al. (2014) conducted creep AE tests on marble and analyzed the influence of different stress levels on internal damage. The AE number and energy release rate suddenly increased when the specimen was subjected to the creep process. Ma et al. (2018) conducted AE tests on coal samples with different moisture contents and studied the influence of moisture content on the creep characteristics of coal. The results showed that the AE characteristics of coal well reflected the evolution process of its creep damage. Zhao et al. (2020) studied the changes in axial stress-strain and AE signal time-frequency parameters of red sandstone specimens under uniaxial compression through the AE event rate, average frequency centroid, peak frequency, and amplitude, and revealed the failure mechanism of red sandstone. Chen et al. (2015) studied the effects of temperature and stress conditions on the creep failure process of granite based on granite creep tests under different temperature and stress states combined with real-time monitoring information of three-dimensional AE. Wu et al. (2016) conducted triaxial creep tests on rock salt and studied the AE characteristics during the first two stages of creep. Jiang et al. (2017) performed long-term and step-loading creep tests of sandstone and collected AE signals throughout the test. The statistical characteristics of the AE energy of the specimen were analyzed by using histogram statistics and maximum likelihood estimation. Shkuratnik et al. (2019) performed simultaneous AE and strain measurements on rock salt specimens and analyzed the changes in the parameters of the salt rock stability and progressive creep stages. Yao et al. (2019) conducted a triaxial creep AE test on sandstones with different water contents and studied the change in the AE RA value at each creep stage.

Overall, the above-mentioned studies have enriched the research results in rock AE experiments. However, the use of AE to understand the creep process of rock masses with prefabricated fissures has rarely been reported till date. The fissures have a significant impact on the creep damage of the rock mass and are one of the critical factors affecting the long-term stability of any engineering project. Therefore, it is necessary to further quantitatively study the effect of fissures on the AE characteristics of rock mass creep.

Therefore, in this study, the effects of prefabricated fissures on the stability and creep process of Triassic sandstone from the Xiaolangdi reservoir area were systematically studied. Under the same test conditions, indoor uniaxial compression creep AE tests were performed on intact sandstone specimens and prefabricated double-fissures sandstone specimens for comparative analysis. The variation characteristics of strain, long-term strength, number of AE events, AE ringing count, AE energy, and RA value of the two specimens were analyzed. The effects of prefabricated fissures on the creep mechanical properties and AE characteristics of sandstone were further obtained. The research results provide a scientific reference for the long-term stability and safety evaluation in rock engineering.

Specimen preparation and test methods

Specimen preparation

The rock blocks used in the test were obtained from the Triassic sandstone in the Dongmiaojia landslide of the Xiaolangdi Reservoir. The sampling site is shown in Figure 1. After arriving in the laboratory, the rock blocks were cut using CNC machine tools. Rectangular parallelepiped specimens with a size of 70 mm × 70 mm × 140 mm (length × width × height) were cut. The uneven deviation of the end surface of the specimen was controlled within the range of ±0.05 mm, and the deviation of the verticality of the end face to the axis was controlled within ±0.25° (Ulusay and Hudson, 2007).

The prefabricated fissures specimen consisted of double-fissures that spanned at an angle through the specimen. The geometric characteristics of the fissures are shown in Figure 2. The length of the fissures was 2a = 30 mm, and the distance between the top ends of the fissures was 2b = 25 mm. The inclination angle of the fissure was $\alpha = 45^{\circ}$, where a is the angle formed by the fissure and the horizontal direction. The inclination angle of the rock bridge was $\beta = 135^{\circ}$, where β is the angle formed between the top line inside the fissure and the horizontal direction.

The prepared intact specimen and the specimen with prefabricated fissures are shown in Figure 3.

Test method

A microcomputer (RLJW-2000) was used to control the rock rheometer and AE tester (PCI-II). Indoor uniaxial compression

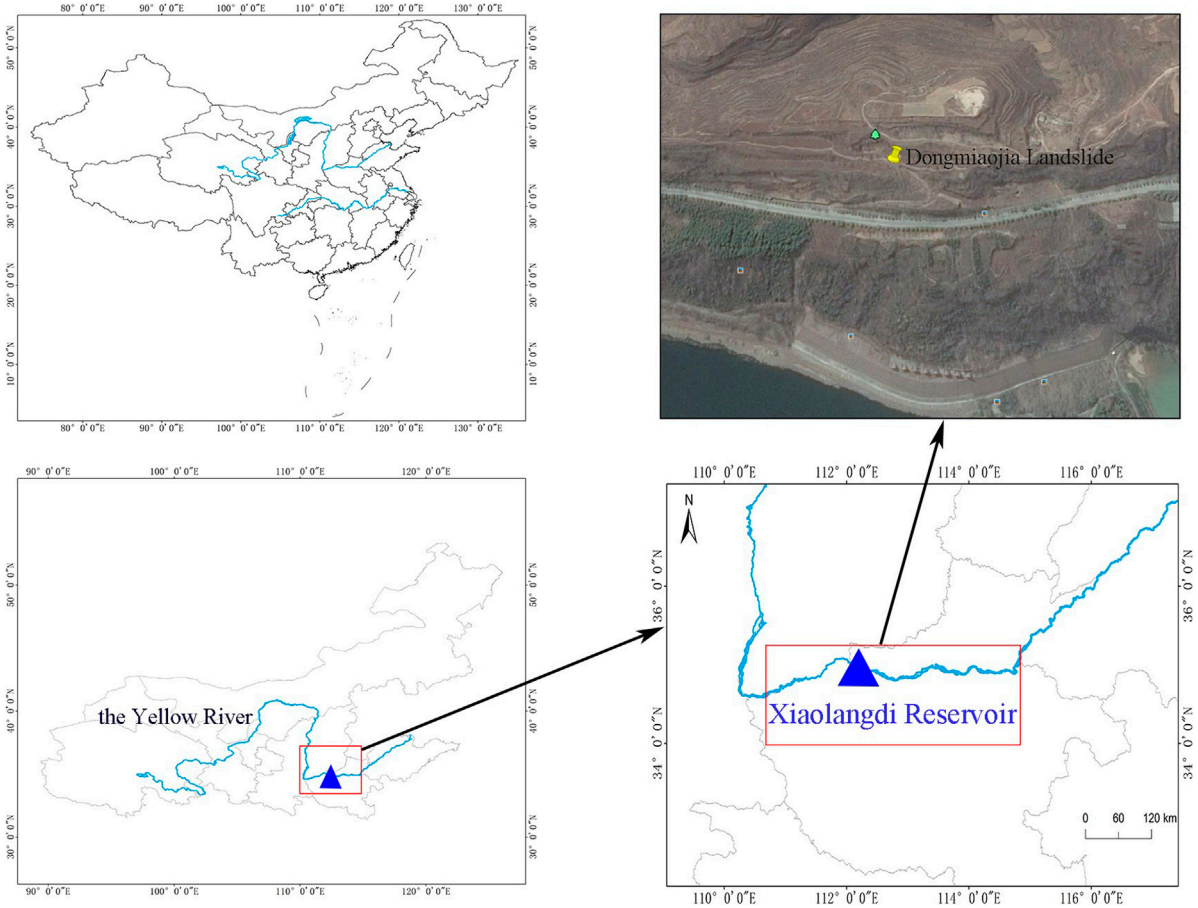

FIGURE 1
Sampling site in the Xiaolangdi Reservoir.

creep AE tests were carried out on the intact and prefabricated double-fissures specimens under the same test conditions.

Axial stress was applied in 15 MPa increments *via* the stepped loading method to compare the creep mechanical properties of the two specimens under the same stress level. Before the failure of the specimen, the axial stress increments were appropriately reduced according to the AE characteristics of the specimen to avoid specimen failure during the loading process. After loading to the first stress level value, the load was kept constant for 2 h and then reloaded to the next stress level value until the specimen underwent creep failure. The stress loading rate was 0.40 kN·s^{-1}. In the test, the deceleration creep stage of the specimen usually lasted about 0.1 h, and the constant creep stage lasted for about 1.0 h after the specimen reached the steady-state creep stage.

Eight R6A AE probes for signal acquisition were used. The probes were arranged in four layers along the side of the specimen to avoid the coplanarity of adjacent probes affecting the acquisition of AE signals. The probe layout is shown in Figure 4. Petroleum jelly was applied to the surface of the AE probe, which was then bonded to the surface of the specimen. The AE threshold was 45 dB, the preamp gain was 40 dB, the specimen rate was one million times s^{-1}, and the filter frequency was in the range of 1 kHz–1 MHz.

The YR-1 rock deformation testing system was used to measure the deformation of the test specimen. The AE and deformation test system used in the experiment is shown in Figure 5.

The stress loading was strictly maintained throughout the experiment. The deformation and AE monitoring were performed simultaneously during the test. The stress, strain, and AE parameters of the two specimens were studied throughout the whole process of change in rock creep change with time. Two sets of parallel tests were performed on the prefabricated fissures specimen, and two sets of parallel comparative tests were also performed on the intact specimens to reduce the dispersion of the test results.

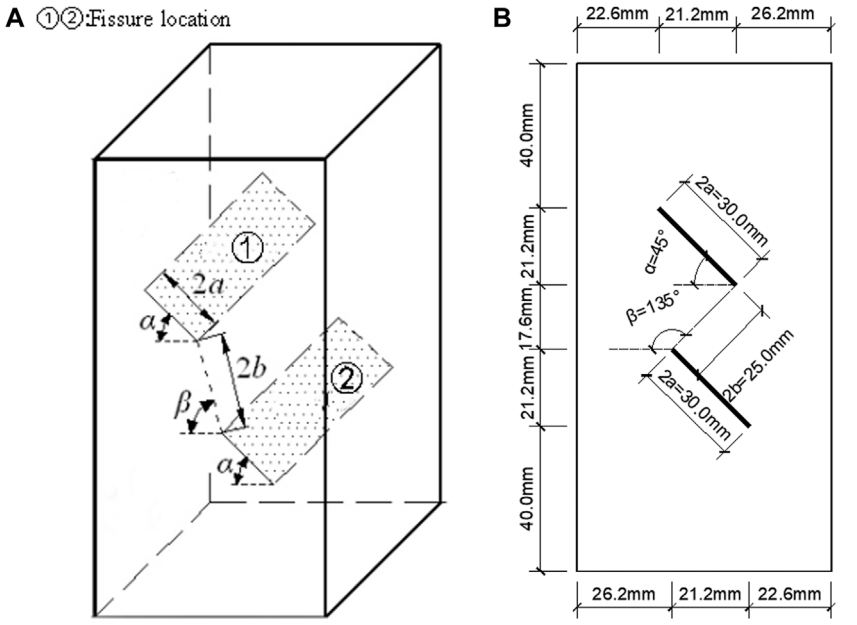

FIGURE 2
The geometric characteristics of the fissures. **(A)** Fissure stereogram. **(B)** Fissure size arrangement.

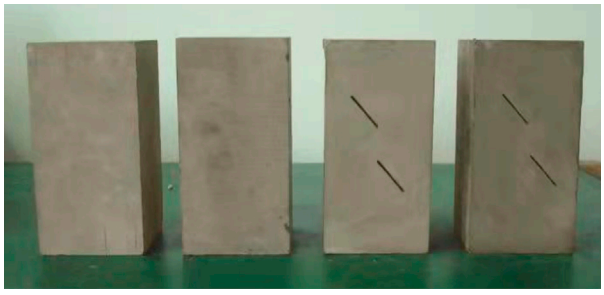

FIGURE 3
Typical sandstone rock specimens without and with fabricated fissures.

Results

Conventional physical and mechanical tests were performed on sandstone specimens. The measured density of the sandstone specimen was 2.64 g·cm^{-3}, the uniaxial compressive strength of the intact specimen was 170.5 MPa, and the uniaxial compressive strength of the prefabricated fissures specimen was 104.9 MPa.

The parallel test results were similar, therefore, representative test results were selected from the intact specimen and the prefabricated fissures specimen for analysis. The graded loading creep curves of the two specimens are shown in Figure 6.

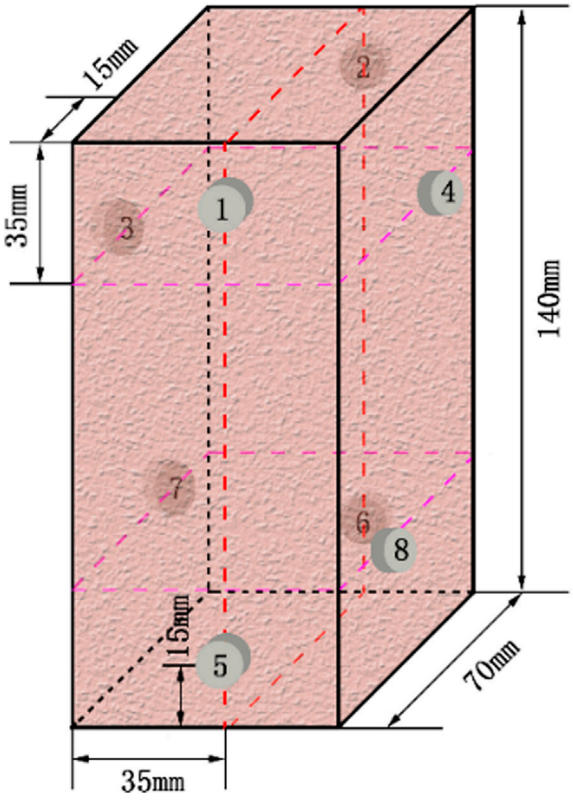

FIGURE 4
Layout of AE sensor probes.

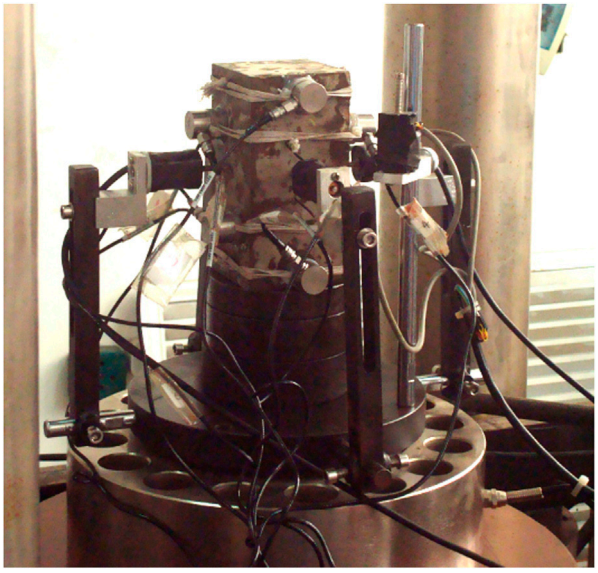

FIGURE 5
AE and deformation test system.

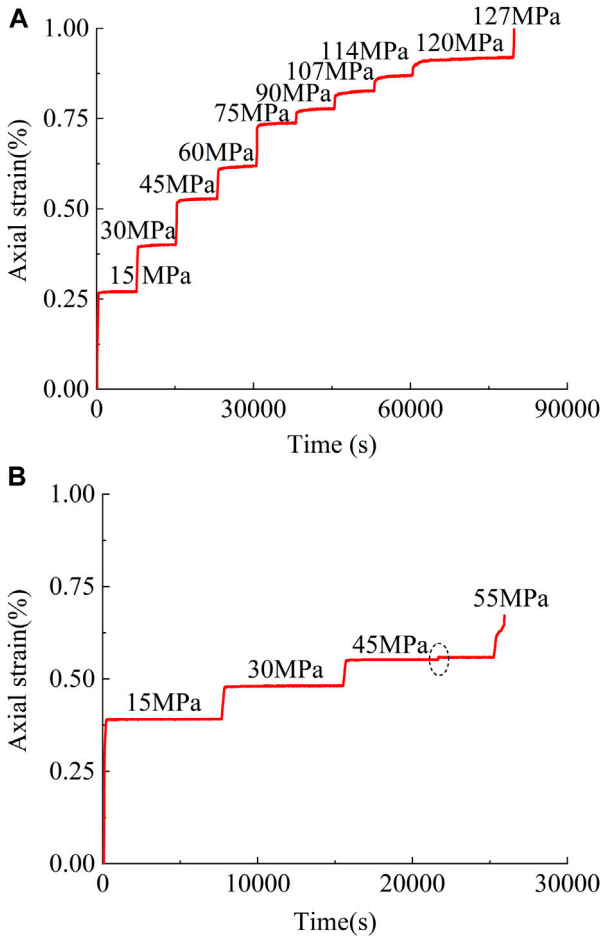

FIGURE 6
Creep curves of sandstone specimen under multi-step loading.**(A)** Intact specimen, and **(B)** prefabricated fissures specimen.

The number on the curve in Figure 6 represents the value of the applied stress level. In the test, 10 and 4 stress levels were applied to the intact specimen and the prefabricated fissures specimen, respectively. The first three stress levels were 15, 30, and 45 MPa for both specimens. Both specimens underwent accelerated creep failure under the action of the last stress level.

Specimen creep mechanical properties

Strain characteristics

According to the hierarchical loading curve shown in Figure 6, Chen's loading method (Tan and Kang, 1980) was used to transform it into a separate loading creep curve, as shown in Figure 7. The creep curves of the two specimens under the first several stress levels can be divided into two stages, namely, deceleration creep and constant velocity creep. Under the last stress level, the creep curve of the specimens can be divided into three stages, namely, decelerating creep, constant velocity creep, and accelerated creep. Noteworthy, the strain curve of the intact rock specimen at the last stress level undergoes the above-mentioned three stages, and the creep time lasts only 91 s. Therefore, the three stages of the strain curve of the intact specimen at the last stress level are not visually displayed in Figure 6A. The creep curves of the intact specimen at all stress levels are relatively straight and smooth, while the creep curves of the prefabricated fissures specimen exhibit a significant step-like sudden increase at a stress level of 45 MPa. Overall, the intact specimen does not undergo the same creep process as the specimen with prefabricated fissures. Under constant stress, the internal cracks in the specimen gradually initiated and expanded over time, and the deformation of the specimen was continuous without a sudden increase. Owing to the influence of prefabricated fissures, stress concentration was likely to occur at the ends of the prefabricated fissure. The secondary microcracks along the ends of prefabricated fissures continued to sprout, expand, overlap, and partially penetrate each other, resulting in a sudden increase in the creep curve.

Under various stress levels, the axial strain of the intact specimen and the prefabricated fissures specimen can be divided into instantaneous strain and creep strain. When the stress is applied at each level, the specimen deforms instantaneously, and then under constant stress, the deformation of the specimen

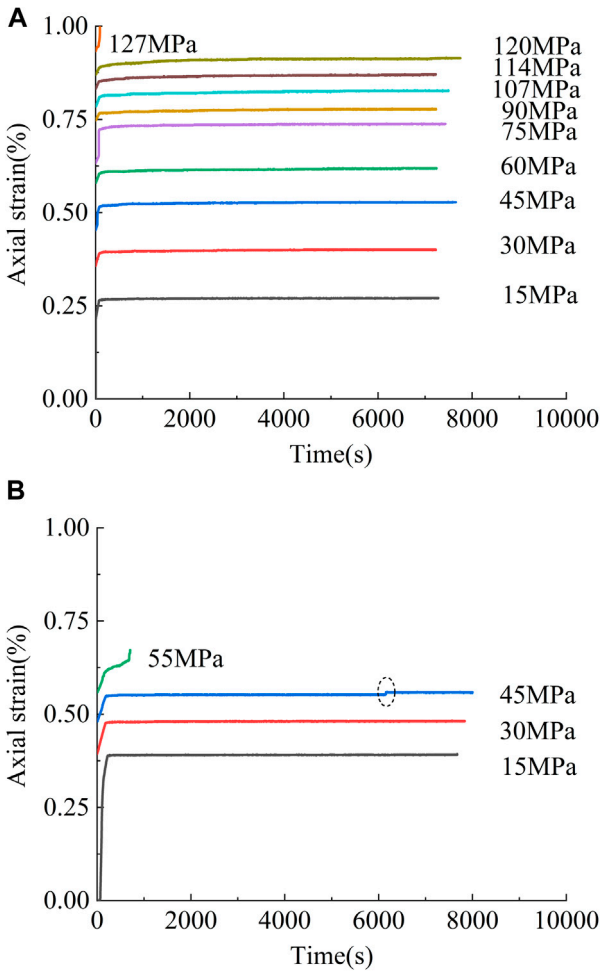

FIGURE 7
Creep Curves of sandstone specimen under respective loading. **(A)** Intact specimen. **(B)** Prefabricated fissures specimen.

increases with time (Yu et al., 2012, Yu et al., 2017). The axial instantaneous strain, creep strain, and total strain of the two specimens under the same first three stress levels are shown in Table 1. Table 1 shows the ratios of the strain of the intact specimen to the strain of the prefabricated fissures specimen.

With the increase in the stress level, the instantaneous strain, creep strain, and total strain of the two specimens gradually increase. Under the same stress level, the instantaneous strain, creep strain, and total strain of the prefabricated fissures specimen are greater than the corresponding values of the intact specimen. The instantaneous strain of the intact specimen is 69.2%–94.4% of the prefabricated fissures specimen, and the creep strain is 57.1%–71.4%, and the total strain is 69.0%–93.8%. Under the same stress level, the creep strain difference between the intact and prefabricated fissures specimen is the largest, followed by the total strain and the instantaneous strain. This indicates that prefabricated fissures have the most significant influence on the creep strain of the specimen.

Long-term strength

Long-term strength is one of the critical parameters for evaluating long-term stability and safety of any engineering project. Researchers have realized the importance of long-term rock strength to long-term stability and safety of some major projects. However, the current research results mainly focus on the long-term strength of macroscopically intact rock specimens, and the long-term strength of rock masses with prefabricated fissures has rarely been investigated. It is necessary to quantitatively study the effect of fissures on the long-term strength of the specimen.

The long-term strength is the maximum axial deviator stress corresponding to the load acting for a long enough time before the creep rupture of a rock specimen occurs (Wan et al., 2021; Zhang et al., 2011). The test results show the comparison between the conventional uniaxial compressive strength and the long-term strength of the two specimens as presented in Table 2. Compared with conventional uniaxial compressive strength, the long-term strengths of the two specimens are reduced to various degrees. The long-term strength of the intact specimen is 70.4% of the conventional uniaxial compressive strength, and the long-term strength of the prefabricated fissures specimen is 42.9% of the conventional uniaxial compressive strength. After considering the time effect, the long-term strength of the

TABLE 1 The instantaneous strain, creep strain, and total strain of specimens under the same stress level.

Stress level value (MPa)	Instantaneous strain (%)			Creep strain (%)			Total strain (%)		
	Intact specimen	Prefabricated fissures specimen	Ratio	Intact specimen	Prefabricated fissures specimen	Ratio	Intact specimen	Prefabricated fissures specimen	Ratio
15	0.267	0.386	0.692	0.004	0.007	0.571	0.271	0.393	0.690
30	0.394	0.475	0.829	0.006	0.009	0.667	0.400	0.484	0.826
45	0.519	0.550	0.944	0.010	0.014	0.714	0.529	0.564	0.938

TABLE 2 Comparison of conventional uniaxial compressive strength and long-term strength of specimens.

Specimen type	Conventional uniaxial compressive strength (MPa)	Long-term strength (MPa)
Intact specimen	170.5	120.0
Prefabricated fissures specimen	104.9	45.0

TABLE 3 Long-term strength of specimens.

Specimen type	Intact specimen (MPa)	Prefabricated fissures specimen (MPa)	Ratio (%)
Long-term strength	120.0	45.0	37.5

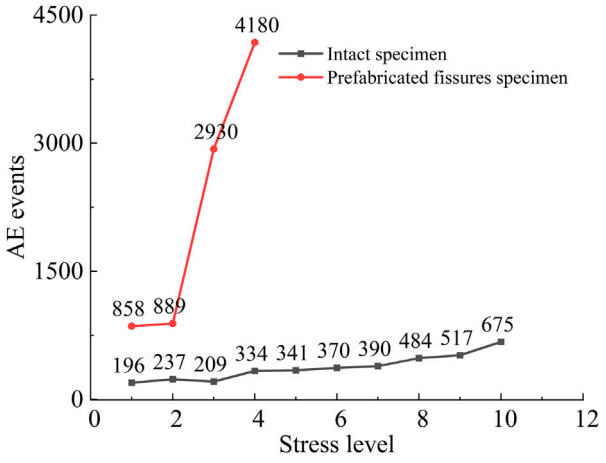

FIGURE 8
AE events of specimens under various stress levels.

specimen is significantly lower than its uniaxial compressive strength. Therefore, compared with the conventional uniaxial compressive strength commonly used in engineering, the long-term strength index of the specimen is more scientific and reasonable for the long-term stability and evaluation of operational safety of a project.

The comparative analysis of long-term strength of the two specimens is presented in Table 3.

Compared with the intact specimen, the long-term strength of the prefabricated fissures specimen is significantly reduced, only 37.5% of the long-term strength of the intact specimen. Long-term strength directly affects the long-term stability and safety of rock engineering. Therefore, the long-term rock strength drop caused by fissures should be addressed in engineering practice.

Acoustic emission characteristics of the specimen

Number of acoustic emission events

The number of AE events and cumulative AE events are parameters that reflect the degree of micro-fracture activity in the rock. Figure 8 shows the number of AE events of the specimen under various stress levels. With an increase in stress level, the number of AE events of the two specimens showed an overall increasing trend, indicating that the higher the stress level results in a greater number of AE events generated by the specimen. The number of AE events of the intact specimen under various stress levels is relatively small, and the curve shows a gentle upward trend with the increase in stress level. However, the number of AE events of the prefabricated fissures specimens under all stress levels is greater than those of the intact specimen.

When the stress levels of the first two levels are relatively small, the difference in the number of AE events between the two specimens is slight, and the curve rises gently. Under the third and fourth stress levels, the curve of the intact specimen still rises gently, while the curve of the prefabricated fissures specimen increases sharply. The number of AE events of the prefabricated fissures specimen increased sharply from 889 to 2,930 under the third stress level. This indicates that the internal fissures rapidly initiate, expand, overlap, and penetrate. Nonetheless, the number of AE events of the intact specimen under this stress level changes slightly. The number of AE events in the prefabricated fissures specimen increased from 2,930 to 4,180 under the fourth stress level, while the number of AE events in the intact specimen only increased from 209 to 334. At the last stress level, the number of AE events of the two specimens reached the maximum values. The number of AE events of the prefabricated fissures specimen was 4,180, which is 6.2 times the number of AE events of the intact specimen of 675. Consequently, the existence of

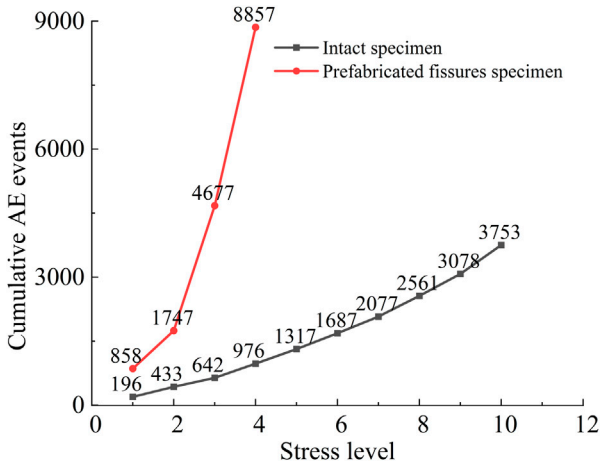

FIGURE 9
Cumulative AE events of specimens under various stress levels.

prefabricated fissures caused more AE events during the creep process of the specimen.

The number of accumulated AE events generated by the specimen under various stress levels is shown in Figure 9. Under various stress levels, the cumulative number of AE events of the intact specimen increases smoothly without sudden increase, with an almost linear slope. In contrast, the number of cumulative AE events of the prefabricated fissures specimen suddenly increases after the second stress level, and the slope of the curve changes significantly. The total number of cumulative AE events generated by the prefabricated fissures specimen reached 8,857, which is 2.4 times the total number of cumulative AE events of the intact specimen of 3,753. As a result, the existence of prefabricated fissures causes more accumulative AE events during the creep process.

In summary, due to the influence of prefabricated fissures, the number of AE events and cumulative AE events generated by prefabricated fissures specimen at various stress levels is significantly higher than the corresponding values of the intact specimen. Prefabricated fissures significantly impact the number of AE events and the number of cumulative AE events. This is attributed to the fact that under constant stress, microcracks easier to initiate, expand, overlap, and penetrate each other at the ends of the prefabricated fissures. In particular, before the final stress level accelerates the creep failure, the number of AE events and the number of cumulative AE events of the prefabricated fissures specimen increase sharply. Therefore, the existence of prefabricated fissures leads to more violent micro-fracture activities inside the specimen and more AE events.

Ringing count and energy

During the creep process, the AE ringing count, AE energy, accumulated AE ringing count, and accumulated AE energy exhibit certain regularities. The axial strain-AE ringing count-cumulative AE ringing count-time curves of the two specimens are shown in Figure 10, and the axial strain-AE energy-cumulative AE energy-time curves of the two specimens are shown in Figure 11. The AE ringing count and AE energy change characteristics are similar during the entire creep process of the two specimens. At each stage of stress loading, the AE ringing count and AE energy of the specimens increase continuously with the increase of time. In contrast, at each stage of constant stress, the AE ringing count and AE energy of the specimens continuously reduce with the increase of time. Therefore, the AE ringing count and AE energy of the specimens exhibit an increase–decrease trend with the increase of time. The AE ringing count and AE energy increase over time under constant stress and show a constant decreasing trend. In the accelerated creep stage during the last stress level, the AE ringing count and the AE energy of the two specimens reach their maximum values. Compared with the intact specimen, the concentration of the AE signal of the prefabricated fissures specimen at this stage is more prominent. AE ringing count and AE energy of the two specimens are presented in Table 4.

The maximum AE ringing count and maximum AE energy of the prefabricated fissures specimen are significantly higher than the corresponding values of the intact specimen. The maximum AE ringing count of the prefabricated fissures specimen is 7.3 times that of the intact specimen, and the maximum AE energy is 3.8 times that of the intact specimen. The prefabricated fissures significantly affect the maximum AE ringing count and maximum AE energy of the specimen.

Furthermore, the change in the cumulative AE ringing count and cumulative AE energy of the two specimens are similar to the change in the specimen strain curve. During the loading stage, the rapid linear rise indicates that the internal cracks of the specimen are constantly initiating and expanding at this stage. As the time prolongs, the curve rises slowly in the constant loading stage, indicating the slowing down of the growth and penetration rate of the internal cracks in the specimen at this stage. The accumulative AE ringing count and accumulative AE energy rise of the prefabricated fissures specimen under the last stress level are significantly larger than the corresponding values of the intact specimen.

The cumulative AE ringing count and cumulative AE energy of the two specimens before the final stress level accelerate the creep failure as presented in Table 4. The

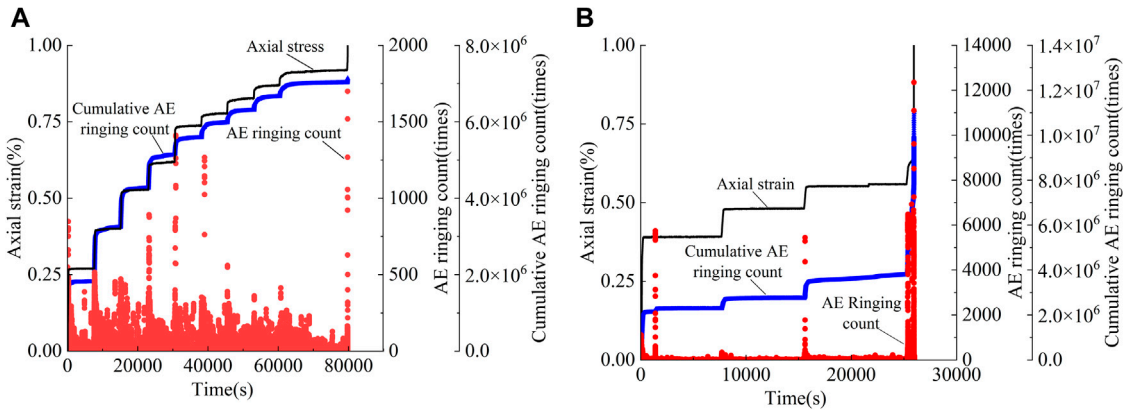

FIGURE 10
Axial strain-AE ringing count-cumulative AE ringing count-time curves of specimens. **(A)**Intact specimen. **(B)** Prefabricated fissures specimen.

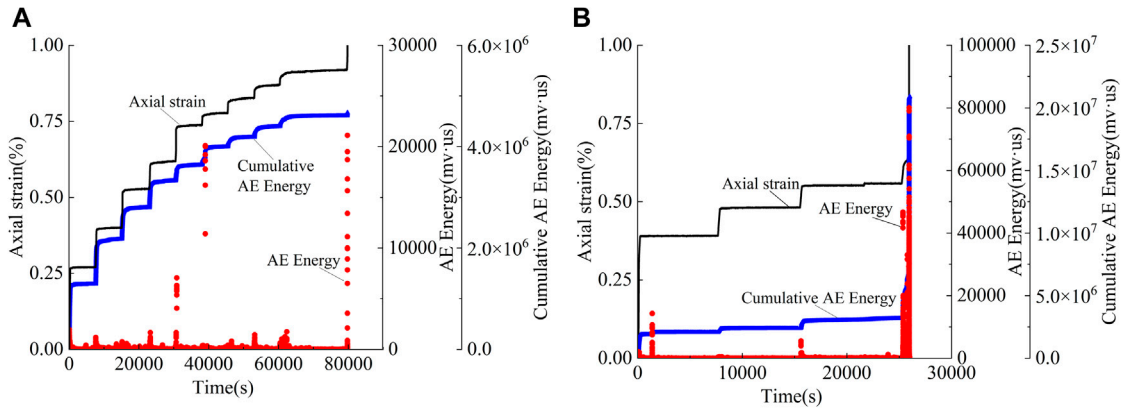

FIGURE 11
Axial strain-AE energy-cumulative AE energy-time curves of specimens. **(A)** Intact specimen. **(B)** Prefabricated fissures specimen.

TABLE 4 AE ringing count and AE energy of specimens under the last stress level.

Specimen type	Maximum AE ringing count (times)	Maximum AE energy (mv·us)	Cumulative AE ringing count (times)	Cumulative AE energy (mv·us)
Intact specimen	1,700	21,112	7.14×10^6	4.67×10^6
Prefabricated fissures specimen	12,348	80,027	1.10×10^7	2.09×10^7

cumulative AE ringing count and cumulative AE energy of the prefabricated fissures specimen are significantly higher than those of the intact specimen. The cumulative AE ringing count of the prefabricated fissures specimen is 1.5 times that of the intact specimen, and the cumulative AE energy is 4.5 times greater. Owing to the effect of prefabricated fissures, stress concentrations are more likely to occur at the fissure ends, and microcracks along the prefabricated fissures ends continue to initiate, expand, overlap, and penetrate, resulting in significantly higher AE ringing count and AE energy for

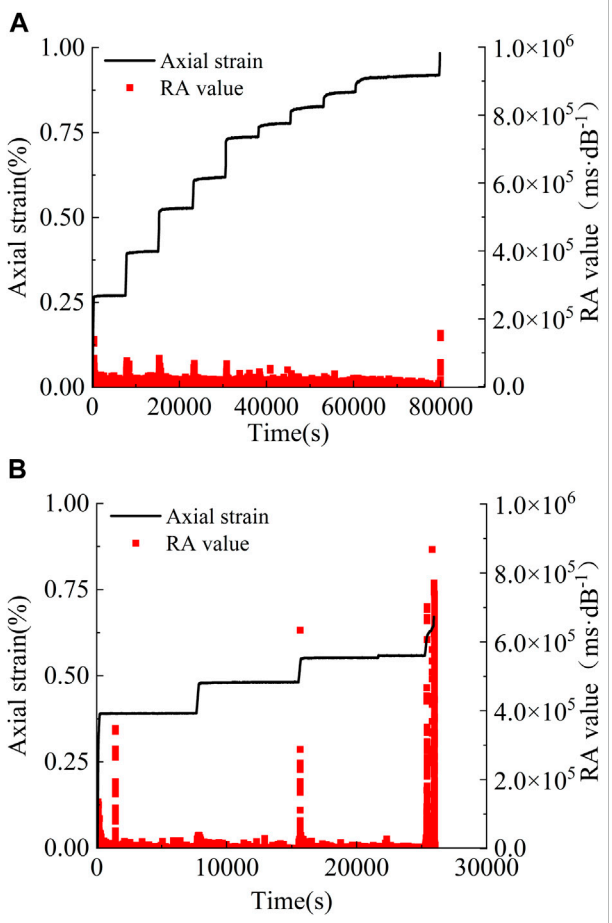

FIGURE 12
Axial strain-RA value-time curve of specimens. **(A)** RA value of Intact specimen. **(B)** RA value of prefabricated fissures specimen.

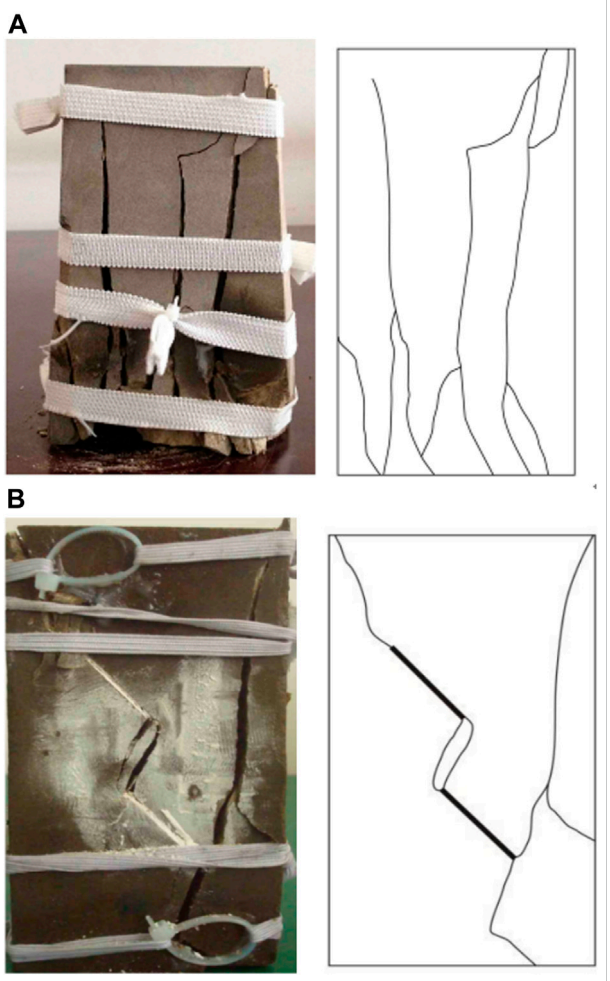

FIGURE 13
Photographs of specimens after creep failure. **(A)** Intact specimen. **(B)**Prefabricated fissures specimen.

the prefabricated fissures specimen than the corresponding values for the intact specimen.

AE RA value

The AE RA-value can characterize the type of cracks inside a material. The parameter RA is defined by Masayasu (2016):

$$RA = \frac{RiseTime\,(RT)}{Amplitude\,(dB)} \tag{1}$$

The unit of RA is ms·dB^{-1}. From a probabilistic statistical perspective, the corresponding relationship between rock AE parameters and crack properties is as follows: an AE signal with a high RA value usually represents the occurrence or development of shear cracks, and an AE signal with a low RA value corresponds to tension cracks.

The axial strain-AE RA-value-time curves of the two specimens under various stress levels are shown in Figure 12. A high RA value and low RA value of the two specimens coexist during the stress loading stage. In the constant stress stage, the RA values of the two specimens are mainly low. Figure 12 exhibits the existence of mutation points in the RA values of the two specimens, which is caused by the continuous initiation, expansion, overlapping, and penetration of microcracks to form a large number of shear microcracks. Figure 12A exhibits that the AE RA-value of the intact specimen is relatively small, all below 157,661.765 (ms·dB^{-1}). The RA value of the specimen significantly increases only during the accelerated creep stage of the final stress level. During the creep process, the cracks generated inside the intact specimen are mainly tensile, and shear cracks are secondary.

Figure 12B demonstrates that the low RA value of the prefabricated fissures specimen is usually less than the low RA

value of the intact specimen. However, the number and values of the high RA value of the prefabricated fissures specimen significantly increase compared to those of the intact specimen. The high RA value of the prefabricated fissures specimen increases sharply compared with that of the intact specimen during the last loading stage. The maximum AE RA-value of the prefabricated fissures specimen is 868,213.333 ($ms{\cdot}dB^{-1}$), which is 5.5 times the RA value maximum of the intact specimen of 157,661.765 ($ms{\cdot}dB^{-1}$). There are 552 RA values for the prefabricated fissures specimen that exceed the maximum RA value of the intact specimen. Analysis of the relationship between the RA value and the type of crack indicates that the type of crack generated inside the prefabricated fissures specimen during the creep process is an obvious mixed tension–shear crack; however, the shear crack is the main one, and the tension crack is the supplement.

Photographs of the two specimens after creep failure are shown in Figure 13. There are more macroscopic tensile cracks (cracks approximately parallel to the axial loading direction) after the creep failure of the intact specimen. Shear cracks appear in the upper and lower parts of the specimen (cracks oblique to the axial loading direction). This is consistent with the observed changes in the internal microcracks of the specimen characterized by the AE RA-value of the specimen. The continuous expansion, overlap, and gradual penetration of the internal microcracks of the specimen eventually lead to the macroscopic cracks of the specimen and the formation of visible damage.

In contrast, the creep damage of the prefabricated fissures specimen mainly occurs around the ends of the prefabricated fissures, and shear cracks are generated at the outer ends of the prefabricated fissures extend to the top and bottom surfaces of the specimens (Wang et al., 2022a; Wang et al., 2022b) (Figure 13B). The shear cracks merge and penetrate with the tensile cracks generated on one side of the specimen. The cracks generated at the inner end of the prefabricated fissures merge to form a tensile–shear composite penetration in the rock bridge area. This is consistent with the change in microcracks characterized by the AE RA-value of the specimen.

In summary, the existence of prefabricated fissures changes the type and number of microcracks inside a specimen, resulting in more shear microcracks. When the macroscopic failure characteristics change, the specimen is more prone to macroscopic shear failure. Identification of the characteristics of internal microcracks in the creep process of the specimen by the RA value is consistent with the macroscopic rupture characteristics of the specimen. Therefore, the RA value, as an essential parameter of AE, shows an excellent guiding significance for characterizing the type of internal microcracks in the process of rock creep.

Conclusion

In this study, uniaxial compression creep acoustic emission (AE) tests were performed on intact sandstone specimens and prefabricated fissures sandstone specimens. The effect of prefabricated fissures on mechanical properties and AE characteristics of sandstone was obtained.

(1) Under the same stress level, the instantaneous strain, creep strain, and total strain of the prefabricated fissures specimen were more significant than the corresponding values of the intact specimen. The difference in creep strain between the two specimens was the largest, followed by the total strain and instantaneous strain. This indicates that the prefabricated fissures exhibit the most significant influence on the creep strain of the specimen, followed by the total strain, and the least on the instantaneous strain.

(2) Compared with the conventional uniaxial compressive strength, the long-term strength of the two specimens was reduced to various degrees. It is more scientific and reasonable to use the rock's long-term strength to evaluate the long-term stability and safety of an engineering project. The long-term strength of the prefabricated fissures specimen was only 37.5% of the long-term strength of the intact specimen. Owing to the influence of prefabricated fissures, the long-term strength of sandstone was significantly reduced. Notably, in engineering applications, the long-term rock strength drop caused by fissures should be critically evaluated.

(3) With the increase in the stress level, the number of AE events of the specimen increases. Under the last stress level, the number of AE events of the specimen reaches its maximum. Furthermore, the number of AE events of the prefabricated fissures specimen was 6.2 times that of the intact specimen at their failure stages. The total number of accumulative AE events of the prefabricated fissures specimen was 2.4 times that of the intact specimen. The number of AE events and cumulative AE events generated by the prefabricated fissures specimen at various stress levels was significantly higher than the corresponding values of the intact specimen. The existence of prefabricated fissures significantly impacts the number of AE events and the number of cumulative AE events in the specimen.

(4) The maximum AE ringing count of the prefabricated fissures specimen was 7.3 times that of the intact specimen, the maximum AE energy was 3.8 times that of the intact specimen, the cumulative AE ringing count was 1.5 times that of the intact specimen, and the cumulative AE energy was 4.5 times that of the intact specimen. The prefabricated fissures significantly affect the maximum AE ringing count, maximum AE energy, cumulative AE ringing count, and cumulative AE energy of specimen.

(5) The intact specimen was dominated by a low RA value, indicating that the microcracks generated by the specimen were mainly tensile cracks, and shear cracks were secondary. Compared with the intact specimen, the number and value of the high RA values of the prefabricated fissures specimen were significantly higher. This indicates that the type of microcracks generated inside the prefabricated fissures specimen was a mixed tension-shear crack dominated by shear cracks. The characteristics of microcracks inside the specimen shown by the RA value were consistent with the macro-fracture characteristics of the specimen. The RA value shows an excellent guiding significance for characterizing the type of internal microcracks in the process of rock creep.

Data availability statement

The original contributions presented in the study are included in the article/Supplementary Material, further inquiries can be directed to the corresponding author.

Author contributions

Conceptualization, HY; conceived and designed the experiments, HY; software, ZZ; validation, GW and ZZ; RN and GC contributed materials and theoretical foundations; writing—original draft preparation, GW; writing—review and editing, HY; All authors have read and agreed to the published version of the manuscript.

Funding

This study was supported by the National Natural Science Foundation of China (Grant No. 51309100), the Opening fund of State Key Laboratory of Geohazard Prevention and Geoenvironment Protection (Chengdu University of Technology) (Grant No. SKLGP 2019K025), the Henan Province Key R&D and Promotion Special (Technology Tackling Key) Project (Grant No. 192102310007), Fund of Innovative Education Program for Graduate Students at North China University of Water Resources and Electric Power, China (Grant No. YK-2021-70).

Conflict of interest

GC was employed by Beijing Engineering Corparation Limited.

The remaining authors declare that the research was conducted in the absence of any commercial or financial relationships that could be construed as a potential conflict of interest.

Publisher's note

References

Chen, X., Wang, S. Z., and Li, L. (2012). Characteristics of fragments of jointed rock mass model under uniaxial compression. *Chin. J. Rock Mech. Eng.* 31 (5), 898–907. (in Chinese). doi:10.1001/2013.jamainternmed.272

Chen, L., Liu, J. F., Wang, C. P., Liu, J., and Wang, J. (2015). Experimental investigation on the creep behaviour of Beishan granite under different temperature and stress conditions. *Eur. J. Environ. Civ. Eng.* 19 (S1), 43–53. doi:10.1080/19648189.2015.1064619

Feng, P., Dai, F., Liu, Y., Xu, N. W., and Du, H. B. (2018). Coupled effects of static-dynamic strain rates on the mechanical and fracturing behaviors of rock-like specimens containing two unparallel fissures. *Eng. Fract. Mech.* 207, 237–253. doi:10.1016/j.engfracmech.2018.12.033

Haeri, H., Shahriar, K., Marji, M. F., and Moarefvand, P. (2014). Experimental and numerical study of crack propagation and coalescence in pre-cracked rock-like disks. *Int. J. Rock Mech. Min. Sci.* 67 (4), 20–28. doi:10.1016/j.ijrmms.2014.01.008

Huang, D., and Huang, R. Q. (2010). Physical model test on deformation failure and crack propagation evolution of fissured rocks under unloading. *Chin. J. Rock Mech. Eng.* 29 (03), 502–512. (in Chinese).

Jiang, D. Y., He, Y., Ouyang, Z. H., Pan, P. Z., Wang, X. S., Xie, K. N., et al. (2017). Acoustic emission energy statistical properties of sandstone during uniaxial creep and its fracture surfaces morphology. *J. China Coal Soc.* 42 (6), 1436–1442. (in Chinese). doi:10.13225/j.cnki.jccs.2016.1101

Li, P., Tang, X. H., Liu, Q. S., and Luo, P. D. (2020). Experimental study on fracture characteristics and strength loss of intermittent fractured quasi-sandstone under freezing and thawing. *Chin. J. Rock Mech. Eng.* 39 (01), 115–125. (in Chinese). doi:10.13722/j.cnki.jrme.2019.0679

Lu, Y. L., Wang, J. G., and Derek, E (2015). Uniaxial strength and failure in sandstone containing a pre-existing 3-D surface flaw. *Int. J. Fract.* 194 (1), 59–79. doi:10.1007/s10704-015-0032-3

Ma, D. P., Zhou, Y., and Liu, C. X. (2018). Creep behavior and acoustic emission characteristics of coal samples with different moisture content. *Acta Geodyn. Geomaterialia* 15 (4), 405–412. doi:10.13168/AGG.2018.0030

Masayasu, O (2016). *Innovative AE and NDT techniques for on-site measurement of concrete and masonry structures*. Springer Netherlands. doi:10.1007/978-94-017-7606-6

Shkuratnik, V. L., Kravchenko, O. S., and Filimonov, Y. L. (2019). Stresses and temperature affecting acoustic emission and rheological characteristics of rock salt. *J. Min. Sci.* 55 (4), 531–537. doi:10.1134/S1062739119045879

Song, Z. Y. (2021). Experimental study on the characteristics of acoustic emission source of rock under uniaxial compression. *IOP Conf. Ser. Earth Environ. Sci.* 791 (1), 012003. doi:10.1088/1755-1315/791/1/012003

Tan, T. K., and Kang, W. F. (1980). Locked in stresses, creep and dilatancy of rocks, and constitutive equations. *Rock Mech.* 13 (1), 5–22. doi:10.1007/BF01257895

Ulusay, R., and Hudson, J. A. (2007). *The complete ISRM suggested methods for rock characterization, testing and monitoring: 1974- 2006*. Compilation arranged by the ISRM Turkish national group: Ankara, Turkey. doi:10.1007/s10064-009-0213-2

Vásárhelyi, B., and Bobet, A. (2000). Modeling of crack initiation, propagation and coalescence in uniaxial compression. *Rock Mech. Rock Eng.* 33 (2), 119–139. doi:10.1007/s006030050038

Wan, Y., Chen, G. Q., Sun, X., and Zhang, G. Z. (2021). Triaxial creep characteristics and damage model for red sandstone subjected to freeze-thaw cycles under different water contents. *Chin. J. Geotechnical Eng.* 43 (08), 1463–1472. (in Chinese). doi:10.11779/CJGE202108011

Wang, G. L., Zhang, L., Wang, Z., Zhang, J. Z., Sun, F., and Qiu, P. Y. (2019). Acoustic-mechanical responses of intact and flaw-contained rock deformation under uniaxial compression: A comparison. *Adv. Civ. Eng.* 2019, 1–12. doi:10.1155/2019/7940923

Wang, Y., Li, J. Z., Zhu, C., and Mao, T. Q. (2022a). Fatigue failure identification using deformation and energy rate for hole-fissure contained granite under freeze–thaw and variable-frequency–variable-amplitude cyclic loads. *Fatigue Fract. Eng. Mat. Struct.* 45 (3), 834–851. doi:10.1111/ffe.13639

Wang, Y., Song, Z. Y., Mao, T. Q., and Zhu, C. (2022b). Macro–meso fracture and instability behaviors of hollow-cylinder granite containing fissures subjected to freeze–thaw–fatigue loads. *Rock Mech. Rock Eng.* 55, 4051–4071. doi:10.1007/s00603-022-02860-5

Wu, C., Liu, J. F., Zhou, Z. W., and Zhuo, Y. (2016). Creep acoustic emission of rock salt under triaxial compression. *Chin. J. Geotechnical Eng.* 38 (S2), 319–323. (in Chinese). doi:10.11779/CJGE2016S2052

Xu, Z. J., Qi, Q. X., Li, H. Y., Zhang, N. B., and Su, R. H. (2014). Acoustic emission characteristics of marble creep damage under different stress levels. *J. China Coal Soc.* 39 (S1), 70–74. (in Chinese). doi:10.13225/j.cnki.jccs.2013.0199

Yang, S. Q., and Jing, H. W. (2011). Strength failure and crack coalescence behavior of brittle sandstone samples containing a single fissure under uniaxial compression. *Int. J. Fract.* 168 (2), 227–250. doi:10.1007/s10704-010-9576-4

Yang, S. Q., Liu, X. R., and Jing, H. W. (2013). Experimental investigation on fracture coalescence behavior of red sandstone containing two unparallel fissures under uniaxial compression. *Int. J. Rock Mech. Min. Sci.* 63, 82–92. doi:10.1016/j.ijrmms.2013.06.008

Yang, C., Huang, D., Cai, R., and Huang, R. Q. (2018). Triaxial unloading creep tests on rock mass with an open and penetrating flaw. *Rock Soil Mech.* 39 (1), 53–62. (in Chinese). doi:10.16285/j.rsm.2015.2821

Yao, Q. L., Zhu, L., Huang, Q. X., Yang, P., and Xu, Z. (2019). Experimental study on the effect of moisture content on creep characteristics of fine-grained feldspar lithic sandstone. *J. Min. Saf. Eng.* 36 (5), 1034–1042. (in Chinese). doi:10.13545/j.cnki.jmse.2019.05.022

Yi, T., Tang, J. X., and Wang, Y. L. (2021). Effect of fracture dip angle and number on mechanical properties and failure modes of rock mass. *Chin. J. Undergr. Space Eng.* 17 (01), 98–106.

Yu, H. C., Li, Y. L., and Liu, H. D. (2012). Comparative study of conventional mechanical, creep and stress relaxation properties of silty mudstone under triaxial compression. *Chin. J. Rock Mech. Eng.* 31 (01), 60–70. (in Chinese). doi:10.3969/j.issn.1000-6915.2012.01.008

Yu, H. C., LiuHuang, H. D. Z. Q., and Shi, G. C. (2017). Experimental study on time-dependent behavior of silty mudstone from the Three Gorges Reservoir Area, China. *KSCE J. Civ. Eng.* 21 (3), 715–724. doi:10.1007/s12205-016-3645-9

Zhang, Q. Y., Yang, W. D., Chen, F., Li, W. G., and Wang, J. H. (2011). Long-term strength and microscopic failure mechanism of hard brittle rocks. *Chin. J. Geotechnical Eng.* 33 (12), 1910–1918. (in Chinese).

Zhao, K., Yang, D. X., Gong, C., Zhuo, Y. L., Wang, X. J., and Zhong, W. (2020). Evaluation of internal microcrack evolution in red sandstone based on time-frequency domain characteristics of acoustic emission signals. *Constr. Build. Mater.* 260, 120435. doi:10.1016/j.conbuildmat.2020.120435

Zhu, L., Zhang, Y., Dong, L., Wu, J. W., Duan, L. Q., and Zhang, L. (2019). Experimental study on acoustic emission characteristics of intermittent jointed rock mass under uniaxial compression. *IOP Conf. Ser. Earth Environ. Sci.* 283 (1), 012015. doi:10.1088/1755-1315/283/1/012015